ACS APPLIED MATERIALS & INTERFACES

RESEARCH ARTICLE

www.acsami.org

Novel, Nanoporous Silica and Titania Layers Fabricated by Magnetron Sputtering

Michael T. P. McCann,[†] Damian A. Mooney,[*,†] Mahfujur Rahman,[†] Denis P. Dowling,[‡] and J. M. Don MacElroy[†]

[†]School of Chemical and Bioprocess Engineering and [‡]School of Electrical, Electronic and Mechanical Engineering, University College Dublin, Belfield Dublin 4, Ireland

ABSTRACT: Composite asymmetric membranes are fabricated through the deposition of submicrometer thick (100 nm) silica (SiO_2) and titania (TiO_2) films onto flat nanoporous silica and zirconia substrates by magnetron sputtering. The deposition conditions for both coating types were systematically altered to determine their influence on the deposited coating morphology and thickness. Ideal He/N_2 gas selectivity was measured for all of the membranes. The TiO_2 coatings, when deposited onto a ZrO_2 support layer with a pore size of 3 nm, formed a long columnar grain structure with average column diameter of 38 nm. A similar columnar structure was observed for TiO_2 coatings deposited onto a SiO_2 support layer with a pore size of 1 nm. Under the same conditions, SiO_2 coatings, deposited onto the same SiO_2 supports, formed a closely packed spherical grain structure whereas, when deposited onto ZrO_2 supports, the SiO_2 coatings formed an open grain structure. The average SiO_2 grain diameter was 36 nm in both cases. This preliminary investigation was aimed at studying the effect of sputtering parameters on the density and morphology of the deposited coatings. For the depositions carried out, the coating material was found to be very dense. However, the presence of grain boundaries resulted in poor ideal He/N_2 separation efficiencies.

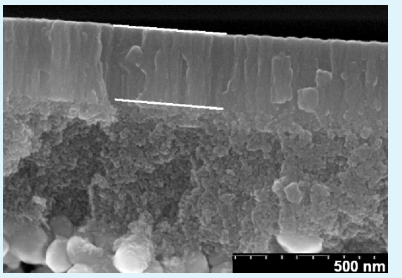

KEYWORDS: thin films, sputtering, nanostructure, membranes

1. INTRODUCTION

Inorganic membranes for gas separation, because of their inherent chemical stability and resistance to high temperature, are useful in applications where the presence of hot gases and corrosive conditions often calls on the use of expensive separation techniques such as distillation, adsorption, or absorption.[1] In order to achieve high levels of selectivity and permeance, which is key to the efficiency of a membrane, an asymmetric configuration is most often used where a thin selective layer is deposited onto a supporting structure. There are several available methods for the deposition of thin coatings, including chemical vapor deposition (CVD),[2] physical vapor deposition (PVD),[3] and sol gel coating.[4] The primary objective of any deposition method (for gas separation applications) is to control the desired layer geometry in order to achieve a high level of selectivity for the given gas mixture to be separated, while also retaining high levels of permeability. These important requirements present a considerable challenge, necessitating the production of membranes with a homogeneous layer, free of pin holes or cracks, crucial for applications where kinetic selectivity is the primary mechanism by which gas separation is achieved.[5,6] In addition, it is important that the membranes are mechanically and hydrothermally stable, as well as of relatively low cost to manufacture.

Magnetron sputtering is a very attractive method for the fabrication of nanostructured materials due to the accurate control it has over the thin film chemistry, thickness, and morphology of deposited layers. Extensive research exists on the use of magnetron sputtering for the industrial manufacture of electrical conduction films and electrically insulating layers for microelectronics, optical films for transmission and reflection, and wear erosion and corrosion resistant coatings.[7−10] Promising results have also been reported on the use of sputtering for the fabrication of dense palladium based membranes for hydrogen separation.[11−13] There are, however, currently very few publications on the utility of sputtering for the production of metal oxide membranes, especially when compared to the array of literature that exists for other techniques, such as CVD and sol−gel.[14] Magnetron sputtering has been used to control the architecture of thin films on mesoporous support layers for applications other than gas separation, including metal oxide sensors, photocatalysis, and ferroelectrics,.[15−19] In terms of membranes for gas separation, recent research has opened up the possibility of the use of magnetron sputtering for gas separation applications.[12,13,20] Successful studies have been conducted by Hoffman et al.[20] on the preparation of gas permeable carbide-derived carbon (CDC) layers, generated by the high temperature (350 °C) chlorination of sputtered TiC layers. These CDC layers (supported on TiO_2/ZrO_2 and Al_2O_3 membranes), with an average pore size of 0.69 nm, demonstrated very good permeation properties for N_2 (4.3×10^{-8} mol $s^{-1}m^{-2}$ Pa^{-1})[20] In other work, Chen and Kitai[21]

Received: September 21, 2010
Accepted: December 22, 2010
Published: January 13, 2011

used magnetron sputtering to deposit SiO_2 layers onto porous anodized alumina. Here, they observed that sputtering resulted in SiO_2 film growth on the surface between the pores of the support, with subsequent deposition leading to increased growth both vertically and laterally, resulting in effective surface pore closure. However, one of the major difficulties in work of this type is the challenge met in adequately characterizing the deposited layers, particularly pore size and pore size distribution.

In this work, the use of magnetron sputtering of both SiO_2 and TiO_2 onto porous $SiO_2/\alpha Al_2O_3$ and $ZrO_2/\alpha Al_2O_3$ is investigated. Both SiO_2 and TiO_2 were chosen as deposition materials by virtue of their potential application as high temperature membrane materials as well as current interest in their application to microelectronics[22,23] and optical devices[23−25] as well as controlled, tribological surfaces.[26,27] The influence of processing conditions such as deposition pressure, target current, substrate bias, target distance, and the use of pulsed and continuous DC power were all investigated with respect to the deposited coatings. The overall objective of this study is to determine the suitability of these magnetron sputtered coatings for high temperature gas-selective membranes.

2. EXPERIMENTAL METHODS

2.1. Support Materials. $SiO_2/\alpha Al_2O_3$ and $ZrO_2/\alpha Al_2O_3$ composites (Inocermic GmbH, Germany) were used as support materials for membrane fabrication. These supports were disk shaped with a diameter of 39.5 mm and thickness of 1 mm (chosen for membrane permeation testing). For both supports, the top layer thickness of SiO_2 or ZrO_2, was between 50 and 100 nm. In terms of average pore sizes, the SiO_2 layer had an average pore size of 1 nm, whereas the ZrO_2 layer had an average pore size of 3 nm. The αAl_2O_3 bottom layer for both substrates had an average pore size of 3 μm, with a thickness of ~1 mm. To prepare the support substrates for deposition, they were first treated in an ultrasonic bath of methanol for 5 min and then in acetone for 20 min. Following this, they were washed in deionized water and dried with clean, dry nitrogen before and after each washing treatment. After cleaning, the supports were heat treated at 400 °C for 12 h (ramp rate = 2 °C/min) in order to remove any carbon residue (arising from the solvent washing) as well as any adsorbed moisture. Prior to the selection of this temperature, a series of experiments were carried out to confirm that the permeation properties and selectivity of the membrane supports was not altered as a result of the heat treatment. The temperature of 400 °C was chosen for heat treatment, as it represented the temperature below which no effect was observed on base layer permeation properties, a key test on changes to underlying structure. Following heat treatment, membranes were used directly to avoid moisture readsorption or contamination.

For the purpose of general characterization and optimization of the processing conditions for coating properties, single crystal silicon wafers (Compart Technology Ltd., UK), with surface roughness values of R_q = 0.93 nm and R_a = 0.74 nm (R_q and R_a are the root-mean-square roughness and average roughness values, respectively), were also used as substrates.

2.2. Magnetron Sputter Deposition. Silica (SiO_2) and titania (TiO_2) coatings were deposited by magnetron sputtering using a Teer Coatings UDP450 closed field unbalanced magnetron sputtering system. The argon plasma is used to systematically bombard a titanium or silicon target in the presence of oxygen to form the corresponding metal oxide coating. A pulsed DC duty factor (ratio of pulse-off time to total pulsing period) of 64% was used, as this value was found to give rise to minimum arcing. The Sparc-LE V DC pulsing unit is fitted with a microarc counting capability. A pure metal titanium target and silicon target (Teer Coatings Ltd., UK) were used for sputtering, and the current applied to the target cathode was controlled by the magnetron drive at 1 and 2 A.

The cylindrical magnetron chamber had a total volume of approximately 0.1 m^3 and was initially evacuated to a pressure of 6×10^{-4} Pa prior to deposition. The argon gas working pressure was varied between 0.1 and 0.4 Pa during deposition. System stability could not be ensured when operated outside of this pressure range. The partial pressure of reactive oxygen gas was accurately controlled to between 2 and 4 std. $cm^3\ min^{-1}$ (SCCM), in order to ensure sputtering in the reactive regime while avoiding target poisoning.[28] The substrate was mounted vertically onto a rotating rack such that the distance between the target and substrate surface could be set between 5 and 17 cm, and the speed of rotation was fixed at 3.1 rpm. Prior to deposition, the substrate was faced away from the target and a current of 0.2 A was applied to the target at a pulsing frequency of 100 kHz in order to etch away any oxide coating that may have formed on the surface of the target between depositions. During the deposition process, an ENI RPG50 power supply unit was used to apply a negative 250 kHz pulsed DC voltage of up to 200 V (maximum) to the substrate. The duty factor of the substrate bias was set at 87.5%.

For each deposition condition, duplicate support materials were used. Following deposition, newly fabricated membranes were transferred to a furnace (Carbolite RF4 200) and subject to a programmed temperature ramp of 2 °C/min up to 400 °C, at which temperature membranes were held for 12 h, before a programmed temperature ramp of 2 °C/min down to 140 °C. Following this, one of the membranes was transferred to the permeation apparatus, with the remaining membrane kept in the furnace at 140 °C until use. Because of the fragile nature of the deposited membrane, care has to be taken when inserting and, particularly, tightening the flange bolts in the permeation cell (see Section 2.3.2 below).

2.3. Material Characterization. One of the greatest challenges associated with studying the deposition of thin layer, porous materials is their characterization. For the case of deposition of these layers onto composite supports, this challenge is made much more difficult. We have investigated a number of techniques, including high resolution transmission electron microscopy (HRTEM) and high sensitivity Brunauer-Emmett-Teller analysis (BET), for this purpose; however, these have all proved inadequate to the task. We have found that the most sensitive (and useful) has been the use of permeation experiments. We have found that, with the correct application of theory, these techniques provide a very sensitive tool in analyzing microstructure. For this reason, they underpin many of the conclusions given below. A number of characterization techniques were employed in this work, with the overall goal of determining the utility of sputtered coatings in high temperature gas separation applications. This is in large part a resto the size of the pores, but more particularly, these are detailed in the following sections.

2.3.1. Gas Permeation Apparatus. Gas permeation measurements were carried out at room temperature using a specially designed and constructed 316 L stainless steel (SS) membrane test apparatus (see Figure 1a). The membrane cell itself (Figure 1b) was designed to accommodate a disk shaped membrane with a diameter of 39.5 mm and a thickness of 1 mm.

Two MKS Baratron gauges (P2, P3) were located downstream of the membrane for the purpose of measuring the increase in pressure with respect to time associated with gas permeating through the membrane. P2 was a type 628D Baratron (FSD 0.1 Torr; accuracy of 0.5% of reading); P3 was a type 622 baratron (FSD 10 Torr; accuracy of 0.25% of reading). A third pressure transducer (P1), also a type 622 baratron (FSD 1000 Torr; accuracy of 0.25% of reading), was located upstream in order to record the initial upstream pressure which remained unchanged throughout the permeance test. Vacuum was achieved by the use of an Edwards RV5 rotary pump and Varian turbo molecular pump, operating in series.

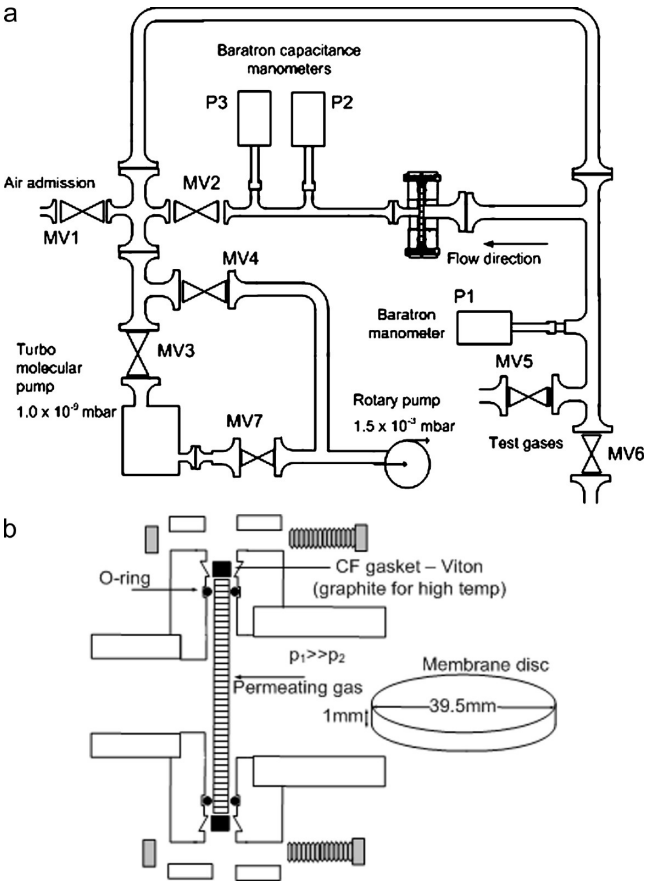

Figure 1. (a) Schematic diagram of permeation rig used for all measurements of gas transport properties; (b) details of flange design for membrane holder used in this experimental work.

2.3.2. Gas Permeation Procedure. In this work, N_2 (99.999%) and He (99.9992%) gases were used for permeation tests. Ideal gas selectivity was determined by administering a fixed pressure of gas upstream of the membrane (from 0.1 to 0.3 bar). The increase in pressure, as measured by P2, P3 was monitored and recorded for a period of 1 min. Equation 1 was used to calculate the permeance (P) where p_2 and p_1 are the upstream and downstream pressures, respectively (see Figure 1a), V is the fixed downstream volume into which the permeating gas flows, and A is the membrane area. A series of permeance experiments on uncoated supports showed that the error in permeance measurements never exceeded ±5%.

$$P = \frac{dp_2}{dt} \times \frac{1}{p_1} \times \frac{V}{ART} \quad (1)$$

For gas flow in porous solids, when the probability of molecule−molecule collisions is negligible compared to molecule−wall collisions, Knudsen diffusion occurs.[29,30] This is the case for microporous and mesoporous solids or when the permeation gas density is low. In this case, the transport flux is given by eq 2. In this equation, P is the permeance (mol s^{-1} m^{-2} Pa^{-1}), ε is the porosity, τ is the tortousity, L is the thickness, and d_p the average pore size of the porous solid. M is the molecular weight of the gas; R is the gas constant, and T is the absolute temperature.

$$P = \frac{\varepsilon d_p}{\tau L} \cdot \left(\frac{8}{9\pi MRT}\right)^{0.5} \quad (2)$$

Equation 2 is based on a simplified model which does not account for the viscous flow contribution toward gas transport and assumes that steric effects may be excluded.

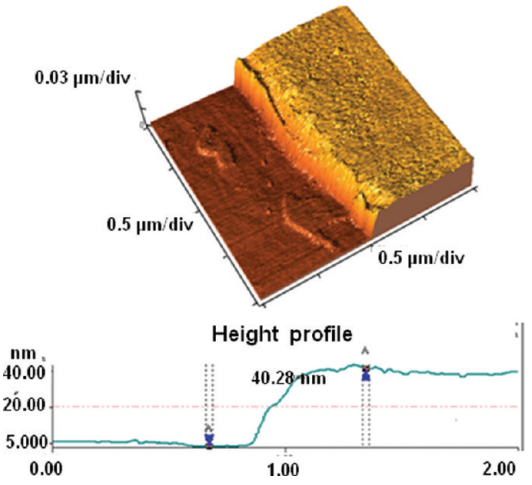

Figure 2. AFM height profile of TiO_2 coating deposited onto silicon wafer.

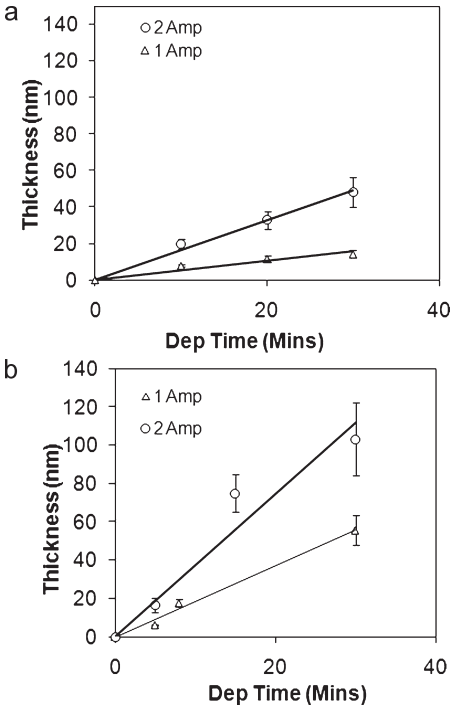

Figure 3. (a) Plot of growth of SiO_2 films (nm) deposited onto silicon wafer using magnetron sputtering as a function of deposition time (minutes); (b) plot of growth of TiO_2 films (nm) deposited onto silicon using magnetron sputtering as a function of deposition time (minutes).

Prior to being mounted onto the membrane holder (shown in Figure 1b), the membranes where heated at 400 °C for a period of 12 h in order to completely remove any adsorbed material from the membrane micropores. For the purposes of comparison, most of the coatings on the membranes evaluated in this study had a thickness of 100 nm (see section 2.3.3 on thickness measurements) so that the effect of film thickness on permeance could be eliminated.

2.3.3. Other Characterization Techniques. Coating thicknesses were determined for films deposited onto silicon wafer substrates, which mounted alongside the membrane samples in the sputtering chamber. The coating thickness was measured using both ellipsometry and atomic force microscopy (AFM) measurements. The latter thickness measurement

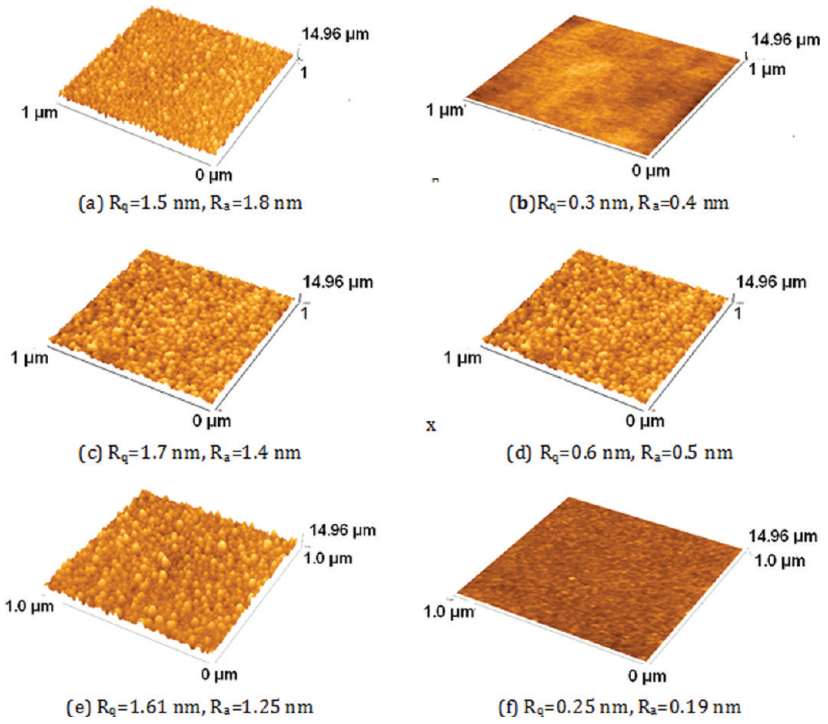

Figure 4. Atomic force microscope (AFM) images of TiO_2 coating surfaces deposited onto silicon wafer at different conditions using magnetron sputtering. (a) 0.4 Pa and (b) 0.1 Pa, (c) no substrate bias, (d) substrate bias voltage of −100 V, and varied target substrate distances of (e) 17 cm and (f) 6 cm.

involved masking a portion of the deposited surface with sharp edge, angled at 45° to the surface such that a profiled edge was obtained[31] (see Figure 2). A Veeco CP-II AFM was used with a 90 μm scanner mounted with a Rotated Tapping-Mode Etched Silicon Probe (RTESP) cantilever probe (tip radius of 10 nm and height of 15 μm). The AFM was operated in noncontact mode. Ellipsometry measurements were carried out using a Woolam M2000 variable angle ellipsometer. A Hitachi S5500 scanning electron microscope (SEM) was used to view the membrane cross sections as well as top surfaces. Due to the nonconductive nature of the membranes, they were first coated in Osmium to aid SEM imaging. Fourier transform infrared spectroscopy (FTIR) spectra were obtained for coated silicon wafers using a Bruker Vertex-70 equipped with a Liquid Nitrogen-cooled Mercury-cadmium-telluride (LN-MCT) detector and KBr beam splitter in order to determine the chemical composition of the deposited layer.

3. RESULTS AND DISCUSSION

3.1. Optimization of Sputtering Parameters. One of the advantages of sputtering in thin-film generation is the control it offers in terms of film thicknesses. In order to assess the rates of film growth during sputtering, a number of deposition experiments were conducted on the silicon wafer substrates in order to determine the influence of deposition conditions on film thickness. The influence of current applied to the titanium and silicon targets on film growth rates of the SiO_2 and TiO_2, respectively, is given in Figure 3a,b. All other processing parameters were held constant, with the target substrate distance set at 10 cm, the working pressure maintained at 2 Pa, and the substrate bias held at 50 V. The growth rates at 1 and 2 A for SiO_2 layers were 1.9 and 0.4 nm/min, respectively, while those for TiO_2 were 3.8 and 1.9 nm/min. These rates are typical for magnetron sputtering deposition and display a good linear fit.

After growth rates were determined, sputtering parameters were optimized to ensure that smooth (layer thickness and morphology) layers were generated. Figure 4 shows AFM images of the different types of surface morphologies of coatings obtained under different conditions of working pressure (panels a and b), substrate bias voltage (panels c and d), and distance between the metal target and the substrate surface (panels e and f). The resulting coating surface was found to be smooth under conditions of low working pressure (1 Pa), high bias voltage (100 V), and closer distance between substrate and target (6 cm). Deposition conducted at varying substrate bias assesses the effect, if any, of deposited species energy,[32] which should lead to a denser coating than would be the case if a lower or zero substrate bias was applied. This has to be balanced with the fact that too large a substrate bias leads to cracking and delaminating of the coating due to the generation and release of residual stress. Reducing the working pressure and/or the lowering of the substrate−target distance was observed to have a similar effect. In terms of the effect of the working pressure on coating morphology, this can be understood by considering the fact that lower working pressures increase the mean-free-path of depositing species, such that less energy absorbing collisions occur as the sputtered particle travels between the target and the substrate surface, i.e., deposition species arrive at the surface with greater energy.

Silica films were found to be more difficult to deposit by dc magnetron sputtering than titania. This was due to the fact that the silicon target (owing to its semiconducting properties) is more susceptible to target poisoning, and consequently, a high degree of arcing was found to occur when high current (2 A) was combined with relatively high working pressures (2 Pa). It was also observed that applying bias to the substrate led to a high degree of arcing. In order to reduce or indeed eliminate arcing the *Sparc Le V* pulsing unit was used. However, even with the *Sparc Le V*, the sputtering parameters had to be tailored to minimize/eliminate the occurrence of arcing. In addition, for the case of

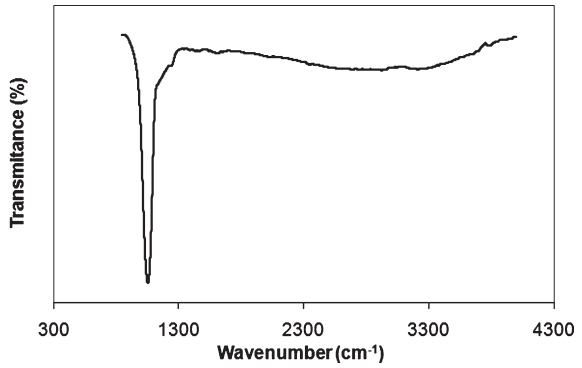

Figure 5. FTIR spectra of SiO_2 coating deposited by magnetron sputtering (deposition conditions are target current of 2 A, pressure of 1 Pa, and distance of 17 cm).

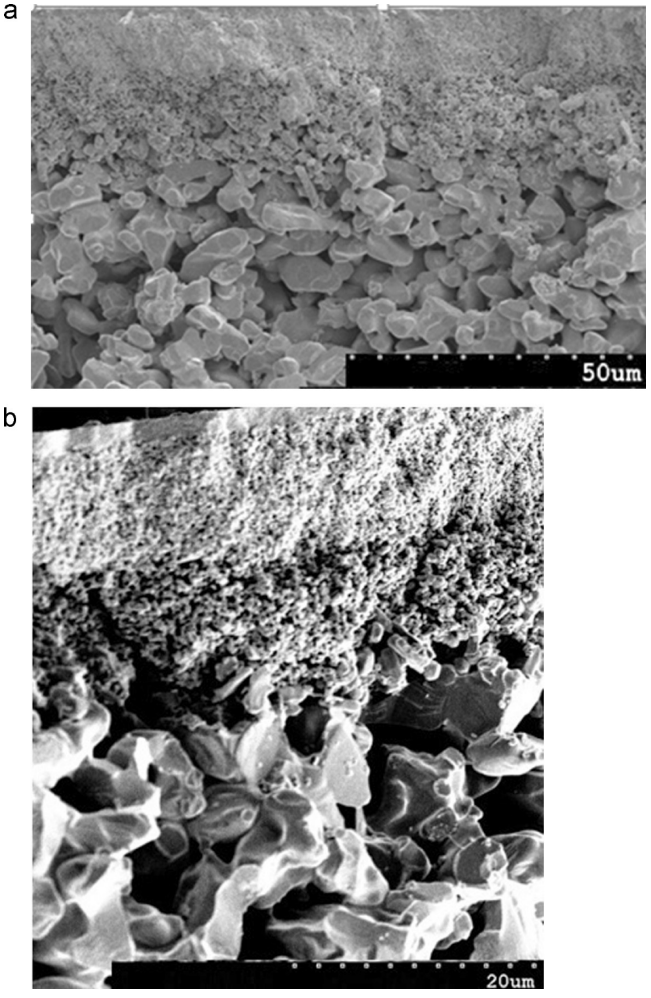

Figure 6. Cross-sectional image of support membranes used in this work. (a) $SiO_2/\alpha Al_2O_3$ composite support, where there top layer is 1 nm SiO_2, supported on 3 μm αAl_2O_3; (b) $ZrO_2/\alpha Al_2O_3$ where the top layer is 3 nm ZrO_2 supported on 3 μm αAl_2O_3.

silica deposition, the normal control mode of the use of optical emissions monitoring (OEM) for reactive gas flow control had to be replaced by the use of traditional mass flow control of oxygen because of the extremely weak light emitted by the silicon plasma (λ = 250−290 nm). In addition to the techniques already mentioned, FTIR was used to examine the chemical functionality of the silica coatings, to verify their purity. Figure 5 shows the spectra for a 100 nm thick coating, with the presence of SiO_2 revealed in the form of the Si−O−Si stretching peak at 1057 cm^{-1}. The stoichiometry of the SiO_2 coating was confirmed by a method reported by Chao et al.[33] where the value of x in the silica from SiO_x ($0 < x < 2$) is related to the shift in the observed peak position relative to the standard peak position of SiO_2 at 1065 cm^{-1}.

3.2. Gas Separation Membranes. Figure 6a,b provides SEM images of the composite $SiO_2/\alpha Al_2O_3$ and $ZrO_2/\alpha Al_2O_3$ supports, respectively, onto which the SiO_2 and TiO_2 coatings were deposited, clearly showing their asymmetric nature. On the basis of the results of section 3.1, depositions were made for a range of deposition parameters on these supports. Under all deposition conditions, the coatings were found to adhere well to the porous support and were thermally stable up to 400 °C. These deposition conditions are shown in Table 2 (for TiO_2 deposition conditions onto ZrO_2) and Table 3 (SiO_2 deposition conditions onto SiO_2), with Figures 7 and 8 showing the corresponding SEM images of the composite membranes, including images of the newly deposited top layer coating. Table 1 summarizes all deposition results in terms of highest values obtained for selectivities for membranes synthesized, including SiO_2 deposition onto ZrO_2 as well as TiO_2 deposited onto SiO_2. Also shown in Table 1 are the selectivities and permeances for the support materials (where measurable).

In Tables 2 and 3, results are also reported for the permeation measurements for N_2 gas, as well as the ideal selectivity, $\alpha_{He/N2}$, for He and N_2. From Table 2, for TiO_2 depositions onto ZrO_2, it can be observed that all fabricated membranes (except when high bias voltage was applied) displayed an ideal He/N_2 selectivity on the order of 2.6, clearly indicative of Knudsen diffusion (see eq 2, where $\alpha_{He/N2} = (M_{N_2} M_{He})^{1/2} = 2.646$) and corresponding N_2 permeances which range from 6.8×10^{-8} mol m^{-2} Pa^{-1} s^{-1} to 16.3×10^{-8} mol m^{-2} Pa^{-1} s^{-1}. For the case of depositions at conditions of high substrate bias, the integrity of the membranes were found to break down, as evidenced by the presence of viscous flow, i.e., where the measured permeance was proportional to the applied upstream pressure. From Table 3, for SiO_2 depositions onto SiO_2, the SiO_2 layer yields an ideal composite membrane selectivity, $\alpha_{He/N2}$, for He over N_2 in the range of 2.5−4.4 and corresponding nitrogen permeance in the range of $0.1-1.28 \times 10^{-8}$ mol m^{-2} Pa^{-1} s^{-1}.

While a TiO_2 layer of 100 nm does not yield any increase in selectivity relative to Knudsen conditions, deposition of a similar thickness of SiO_2 at a working pressure of 0.1 and target current of 2 A leads to a membrane He/N_2 selectivity of $\alpha_{He/N2} = 3.9$ and a considerable reduction in nitrogen permeance. The nitrogen permeance of the $SiO_2/ZrO_2/\alpha Al_2O_3$ composite membrane was 0.11×10^{-8} mol m^{-2} Pa^{-1} s^{-1} which is approximately 74 times smaller than that for the $TiO_2/ZrO_2/\alpha Al_2O_3$ composite membrane which had a nitrogen permeance of 8.1×10^{-8} mol m^{-2} Pa^{-1} s^{-1}. The difference is much less in the case of deposition onto SiO_2 for which the nitrogen permeance of the $SiO_2/SiO_2/\alpha Al_2O_3$ composite membrane was 0.10×10^{-8} mol m^{-2} Pa^{-1} s^{-1} which is approximately 10 times smaller than that for the $TiO_2/SiO_2/\alpha Al_2O_3$ which had a nitrogen permeance of 0.98×10^{-8} mol m^{-2} Pa^{-1} s^{-1}.

The SEM images provide an insight as to the possible reasons for the differences in permselectivity. The Titania coatings shown in Figure 7c show a distinctive columnar structure when compared

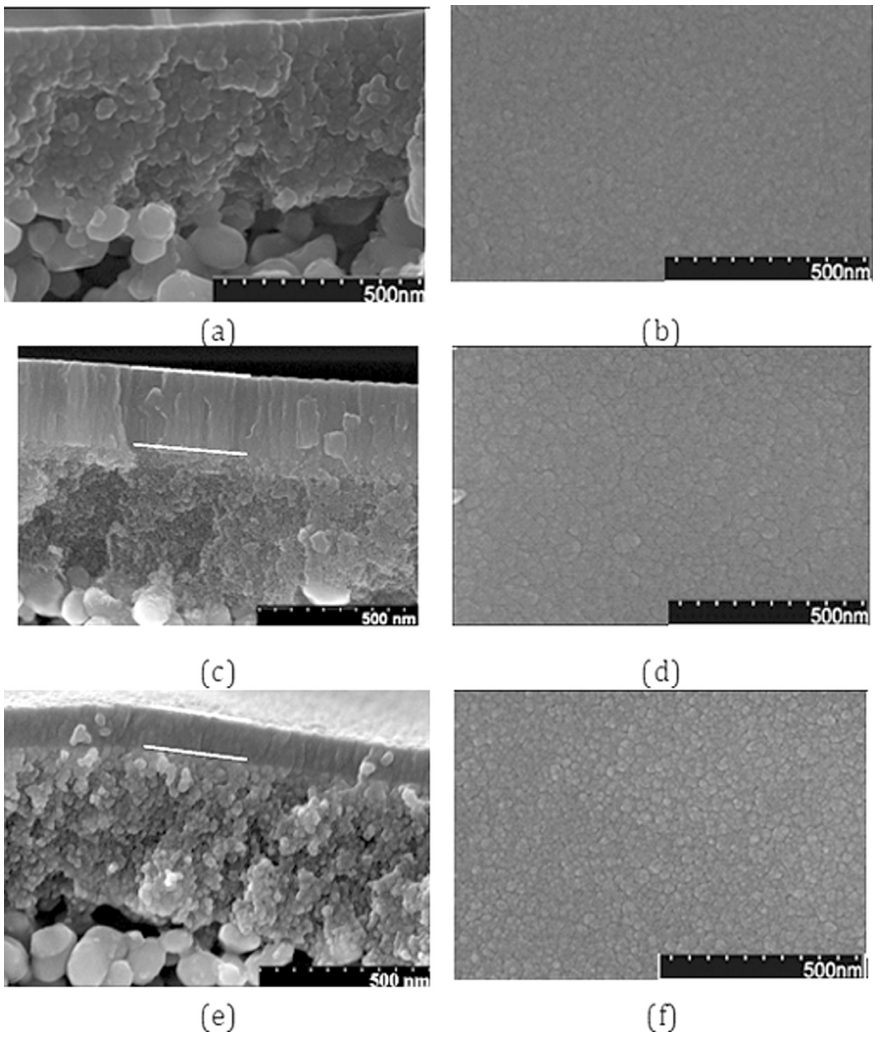

Figure 7. SEM images showing uncoated ZrO_2 membrane supports (a) cross-section, (b) top; supports with TiO_2 coating deposited by magnetron sputtering, (c) cross-section, (d) top and 100 nm thick SiO_2 coating [(e) cross-section, (f) top].

to the more amorphous structure of the ZrO_2 support material shown in Figure 7a. The columnar structure was not observed for depositions onto smooth silicon wafer surface, and for this reason, it may be postulated that the granular structure, for the depositing conditions investigated, arises from the presence of pores on the support surface. Although the columnar structure was not as obvious for deposition of TiO_2 onto the SiO_2 support with 1 nm pores, as can be seen when comparing Figures 7c and 8e, the structure of such a coating appears to consist of vertical arrayed granules interspaced with spherical subdomains as shown in Figure 8e. The distinct columnar structure, with grain boundaries extending from the surface right down to the support layer, was not observed for the SiO_2 depositions which resulted in coatings consisting of open and packed grains as shown in Figures 7e and 8c, respectively. Packed grains create a more tortuous path for gas flow. The packed grains were observed when SiO_2 was deposited onto porous SiO_2 with a pore size of 1 nm as shown in Figure 7e. The open grains were observed when SiO_2 was deposited onto porous ZrO_2 with a pore size of 3 nm as shown in Figure 8c. The permeation data and SEM images presented for the deposition of TiO_2 and SiO_2 onto porous ZrO_2 and SiO_2 present sufficient data to infer that the sputtered SiO_2 coating, which has less of a tendency for columnar structures than sputtered TiO_2, results in lower rates of permeance than that of TiO_2 due to a higher layer tortousity. In addition, it may be postulated that the higher selectivity of the SiO_2 coated membrane is due to a smaller average pore size as a result of the compaction of layer grains. SEM images show the TiO_2 columns (Figure 7c,d) to have an average diameter of 38 nm $\pm$ 9 nm and the TiO_2 grains (Figure 8e,f)) to have a smaller diameter of 32 nm $\pm$ 7 nm whereas the SiO_2 spherical grains (Figures 7e,f and 8b,d) were found to have a diameter of 36 nm $\pm$ 9 nm.

According to simple models for gas transport in porous membranes, it is generally accepted that, for asymmetric membranes, the individual permeance of two layers may be added reciprocally to yield the total permeance P_{tot} as described by eq 3.

$$\frac{1}{P_{tot}} = \frac{1}{P_1} + \frac{1}{P_2} \quad (3)$$

From this expression and the data listed in Table 1, helium and nitrogen permeances of the SiO_2 deposited layer were calculated to be 0.38×10^{-8} mol m^{-2} Pa^{-1} s^{-1} and 0.098×10^{-8} mol m^{-2} Pa^{-1} s^{-1}, respectively, which yields an ideal He/N_2 selectivity of the α = 3.9. In the case of TiO_2 deposited onto a SiO_2 support, the helium and nitrogen permeances of the coating layer were calculated to be 3.86×10^{-8} mol m^{-2} Pa^{-1} s^{-1}

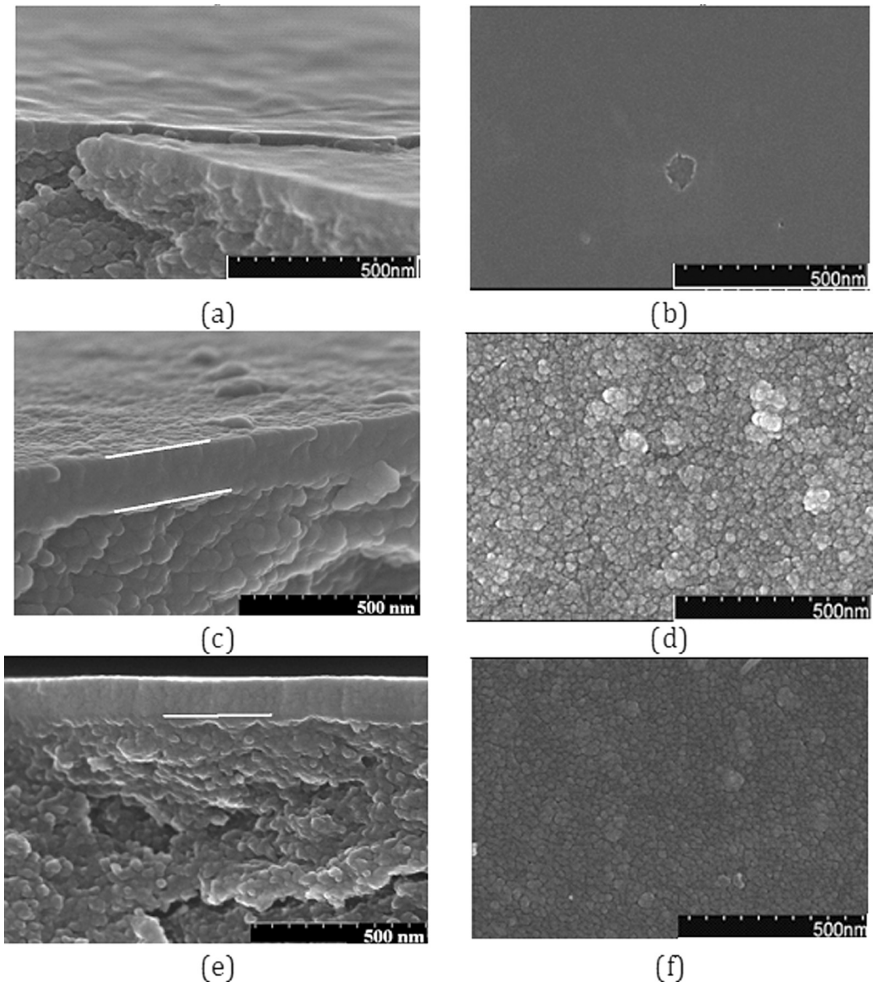

Figure 8. SEM images showing uncoated SiO_2 membrane supports [(a) cross-section, (b) top]; supports with SiO_2 coating deposited by magnetron sputtering [(c) cross-section, (d) top] and TiO_2 coating [(e) cross-section, (f) top].

Table 1. Results for Ideal He/N_2 Selectivities and Permeances for Combinations of Substrates and Coatings Deposited in This Work[a]

support	coating	He/N_2 selectivity	He permeance $\times 10^8$ (mol/s/m^2/Pa)	N_2 permeance $\times 10^8$ (mol/s/m^2/Pa)
			Support	
$ZrO_2/\alpha Al_2O_3$[b]	none			
			Composite Membrane (Coating)	
	TiO_2	2.6	21.4	8.1
	SiO_2	3.3	0.36	0.11
			Support	
$SiO_2/\alpha Al_2O_3$	none	4.3	6.8	1.5
			Composite Membrane (Coating)	
	TiO_2	2.6	2.47	0.98
	SiO_2	3.9	0.42	0.10

[a] Permeation values of the $ZrO_2/\alpha Al_2O_3$ substrate are outside of the detection limits of the permeation apparatus. [b] The maximum detection limit of the apparatus is 1×10^{-5} mol/s/m^2/Pa, and therefore, the permeance for these membranes could not be measured. The nominal pore size (according to the manufacturer) of the ZrO_2 support was 3 nm, and therefore, it would be expected that the He/N_2 would be equal to 2.6, indicative of Knudsen diffusion.

and 2.65×10^{-8} mol m^{-2} Pa^{-1} s^{-1}, respectively, which yields an idea He/N2 selectivity of approximately $\alpha = 1.5$. The observed permeance data implies that TiO_2 coated membranes exhibit higher gas permeances, indicative of the larger average pore size which results from loosely packed grains. The grain size of the SiO_2 coating is of a similar order of magnitude to that of the TiO_2

Table 2. Conditions Used During the Deposition of TiO_2 Coatings onto $ZrO_2/\alpha Al_2O_3$ Using Magnetron Sputtering and Comparison of Ideal He/N_2 Selectivity and Permeance Achieved for These Conditions

parameter	deposition time (mins)	power supply	substrate −target distance (cm)	working pressure (Pa)	substrate bias (V)	target current (A)	target output voltage (V)	αHe/N2	N_2 permeance × 10^8 (mol/s/m^2/Pa)
pulsed dc	20	PDC	6	0.2	50	2	202	2.57	16.3
continuous dc	20	DC	6	0.2	50	2	375	2.59	6.8
pressure	20	PDC	6	0.1	50	2	210	2.64	8.1
bias	20	PDC	6	0.2	200	2	202	viscous flow[a]	
target distance	20	PDC	10	0.2	50	2	200	2.54	8.7
target current	20	PDC	6	0.2	50	4	222	2.59	8.9
deposition time	40	PDC	6	0.2	50	2	288	2.61	12.3

[a] With viscous flow permeance changes with applied upstream pressure.

Table 3. Conditions Used during the Deposition of SiO_2 Coatings onto $SiO_2/\alpha Al_2O_3$ Using Magnetron Sputtering and Comparison of Ideal He/N_2 Selectivity and Permeance Achieved for These Conditions

parameter	substrate−target distance (cm)	working pressure (Pa)	substrate bias (V)	target current (A)	target output voltage (V)	αHe/N2	N_2 permeance ×10^8 (mol/s/m^2/Pa)
target distance	17	0.1	0	2	171	3.9	0.1
bias	6	0.2	50	2	433	2.5	0.25
target current	17	0.1	0	1	199	4.4	1.28
pressure	6	0.3	0	2.5	267	3.4	0.2

coating grain, as indicated by the SEM images where the average grain sizes are 38 and 36 nm, respectively. However, the He/N_2 selectivities $\alpha = 3.9$ for SiO_2 vs $\alpha = 1.5$ for the TiO_2 coating indicate that the SiO_2 grains are more tightly packed than those of TiO_2. The grain spacing of the TiO_2 coating is of a level which results in transitional or viscous flow as the He/N_2 selectivity is less than 2.6 and the SiO_2 grain spacing is of a level where steric effects play a role in the gas transport mechanism as He/N_2 selectivity is greater than 2.6.

4. CONCLUSION

Silica and titania films were deposited onto porous SiO_2 and ZrO_2 support membranes by reactive magnetron sputtering. The sputtering process was optimized to accurately control membrane thickness, chemistry, and morphology. The corresponding permeance of N_2 and He was measured at room temperature for both deposited coatings. The presence of a columnar structure and inherent grain boundaries led to poor separation efficiencies. This was due to the high surface roughness and presence of pores on the surface support layer. In order to conclude on the feasibility of magnetron sputtering as a potential method for the production of microporous membranes, a more comprehensive study covering a wider range of individual process parameters is required in order to find those parameters that lead to denser coatings with more compact grain boundaries. Due to the accurate control of membrane thickness and chemistry and ease of scale-up, magnetron sputtering may present an ideal low cost method for fabrication of microporous or dense nonporous membranes which may be used as a coating for reducing base-layer permeance rates.

AUTHOR INFORMATION

Corresponding Author

*E-mail: damian.mooney@ucd.ie.

ACKNOWLEDGMENT

We would like to thank Dr. Janusz Bucki and his co-workers at the Materials Science Department at Warsaw University of Technology for their assistance in providing the SEM images. The financial support of the EU Sixth Framework Programme is gratefully acknowledged (Grant No.: NMP3- NMP3-CT-2005-014032).

REFERENCES

(1) Bredesen, R.; Jordal, K.; Bolland, A. *Chem. Eng. Process.* **2004**, *43*, 1129–1158.
(2) Gu, Y. F.; Hacarlioglu, P.; Oyama, S. T. *J. Membr. Sci.* **2008**, *310*, 28–37.
(3) Jayaraman, V.; Lin, Y. S. *J. Membr. Sci.* **1995**, *104*, 251–262.
(4) da Costa, J. C. D.; Lu, G. Q.; Rudolph, V.; Lin, Y. S. *J. Membr. Sci.* **2002**, *198*, 9–21.
(5) MacElroy, J. M. D. *Mol. Phys.* **2002**, *100*, 2369–2376.
(6) Cuffe, L.; MacElroy, J. M. D.; Tacke, M.; Kozachok, M.; Mooney, D. A. *J. Membr. Sci.* **2006**, *272*, 6–10.
(7) Mohamed, S. H.; Kappertz, O.; Pedersen, T. P. L.; Drese, R.; Wuttig, M. *Phys. Status Solidi A: Appl. Res.* **2003**, *198*, 224–237.
(8) Eufinger, K.; Poelman, D.; Poelman, H.; De Gryse, R.; Marin, G. B. *Appl. Surf. Sci.* **2007**, *254*, 148–152.
(9) Huang, C. C.; Tang, J. C.; Tao, W. H. *Sol. Energy Mater. Sol. Cells* **2004**, *83*, 15–28.
(10) Stamate, M. D. *Thin Solid Films* **2000**, *372*, 246–249.
(11) Thomann, A. L.; Rozenbaum, J. P.; Brault, P.; Andreazza-Vignolle, C.; Andreazza, P. *Appl. Surf. Sci.* **2000**, *158*, 172–183.
(12) Huang, Y.; Dittmeyer, R. *J. Membr. Sci.* **2007**, *302*, 160–170.
(13) Mekonnen, W.; Arstad, B.; Klette, H.; Walmsley, J. C.; Bredesen, R.; Venvik, H.; Holmestad, R. *J. Membr. Sci.* **2008**, *310*, 337–348.
(14) Lin, Y. S.; Kumakiri, I.; Nair, B. N.; Alsyouri, H. *Sep. Purif. Methods* **2002**, *31*, 229–379.
(15) Gorokh, G.; Mozalev, A.; Solovei, D.; Khatko, V.; Llobet, E.; Correig, X. *Electrochim. Acta* **2006**, *52*, 1771–1780.
(16) Turkevych, I.; Pihosh, Y.; Goto, A.; Kasahara, A.; Tosa, A.; Kato, S.; Takehana, K.; Takamasu, T.; Kido, G.; Koguchi, N. *Thin Solid Films* **2008**, *516*, 2387–2391.

(17) Johnson, P. L.; Teeters, D. *Solid State Ionics* **2006**, *177*, 2821–2825.
(18) Mishina, E. D.; Stadnichuk, V. I.; Sigov, A. S.; Golovko, Y. I.; Mukhorotov, V. M.; Nakabayashi, S.; Masuda, H.; Hashizume, D.; Nakao, A. *Phys. E* **2004**, *25*, 35–41.
(19) Ding, D. Y.; Chen, Z.; Lu, C. *Sens. Actuators, B: Chem.* **2006**, *120*, 182–186.
(20) Hoffman, E. N.; Yushin, G.; Wendler, B. G.; Barsoum, M. W.; Gogotsi, Y. *Mater. Chem. Phys.* **2008**, *112*, 587−591.
(21) Chen, F.; Kitai, A. H. *Thin Solid Films* **2008**, *517*, 622–625.
(22) Hurley, R. E.; Gamble, H. S. *Vacuum* **2003**, *70*, 131–140.
(23) Tang, H.; Prasad, K.; Sanjines, R.; Schmid, P. E.; Levy, F. *J. Appl. Phys.* **1994**, *75*, 2042–2047.
(24) Asanuma, T.; Matsutani, T.; Liu, C.; Mihara, T.; Kiuchi, M. *J. Appl. Phys.* **2004**, *95*, 6011–6016.
(25) Ternon, C.; Gourbilleau, F.; Portier, X.; Voivenel, P.; Dufour, C. *Thin Solid Films* **2002**, *419*, 5–10.
(26) Wu, W. F.; Chiou, B. S. *Appl. Surf. Sci.* **1996**, *99*, 237–243.
(27) Krishna, D. S. R.; Sun, Y. *Surf. Coat. Technol.* **2005**, *198*, 447–453.
(28) Sproul, W. D.; Christie, D. J.; Carter, D. C. *Thin Solid Films* **2005**, *491*, 1–17.
(29) Knudsen, M. *Kinetic Theory of Gases: Some Modern Aspects*, 3rd ed.; London: Methuen & Co. Ltd., 1950.
(30) Cunningham, R. E., Williams, R. J. J. *Diffusion in gases and porous media*; Plenum Press: New York, 1980.
(31) Guillermo Acosta, D. D. A.; Davis, R. C. *A Technique for Measuring the Thin Film Thickness of Ultrathin Metallic Thin Films, 4-20 nm, using Atomic Force Microscopy*; Summer News Bulletin of the Society of Vacuum Coaters, 2005; pp 34−38.
(32) Kelly, P. J.; Beevers, C. F.; Henderson, P. S.; Arnell, R. D.; Bradley, J. W.; Backer, H. *Surf. Coat. Technol.* **2003**, *174*, 795–800.
(33) Chao, S. S.; Takagi, Y.; Lucovsky, G.; Pai, P.; Custer, R. C.; Tyler, J. E.; Keem, J. E. *Appl. Surf. Sci.* **1986**, *26*, 575−583.